# Experimental and Theoretical Studies of the Reaction of the OH Radical with Alkyl Sulfides: 3. Kinetics and Mechanism of the OH Initiated Oxidation of Dimethyl, Dipropyl, and Dibutyl Sulfides: Reactivity Trends in the Alkyl Sulfides and Development of a Predictive Expression for the Reaction of OH with DMS

**M. B. Williams,[†] P. Campuzano-Jost,[‡] and A. J. Hynes***

*Division of Marine and Atmospheric Chemistry, Rosenstiel School of Marine and Atmospheric Science at the University of Miami, 4600 Rickenbacker Causeway, Miami, Florida 33149*

**A. J. Pounds**

*Department of Chemistry, Mercer University, 1400 Coleman Avenue, Macon, Georgia 31207*

*Received: February 5, 2009; Revised Manuscript Received: April 20, 2009*

A pulsed laser photolysis−pulsed laser-induced fluorescence technique has been employed to measure rate coefficients for the OH-initiated oxidation of dimethyl sulfide (DMS), its deuterated analog (DMS-$d_6$), dipropyl sulfide (DPS), and dibutyl sulfide (DBS). Effective rate coefficients have been measured as a function of the partial pressure of $O_2$ over the temperature range of 240−295 K and at 200 and 600 Torr total pressure. We report the first observations of an $O_2$ enhancement in the effective rate coefficients for the reactions of OH with DPS and DBS. All observations are consistent with oxidation proceeding via a two-channel oxidation mechanism involving abstraction and addition channels. Structures and thermochemistry of the DPSOH and DBSOH adducts were calculated. Calculated bond strengths of adducts increase with alkyl substitution but are comparable to that of the DMSOH adduct and are consistent with experimental observations. Reactivity trends across the series of alkyl sulfide ($C_2$−$C_8$) reactions are analyzed. All reactions proceed via a two-channel mechanism involving either an H-atom abstraction or the formation of an OH adduct that can then react with $O_2$. Measurements presented in this work, in conjunction with previous measurements, have been used to develop a predictive expression for the OH-initiated oxidation of DMS. This expression is based on the elementary rate coefficients in the two-channel mechanism. The expression can calculate the effective rate coefficient for the reaction of OH with DMS over the range of 200−300 K, 0−760 Torr, and 0−100% partial pressure of $O_2$. This expression expands on previously published work but is applicable to DMS oxidation throughout the troposphere.

## Introduction

The use of structure additivity relationships has proven to be a powerful tool in rationalizing the observed reactivity of many classes of organic compounds with the OH radical.[1−3] Although it is a simple, empirical technique, it allows the rationalization and prediction of the rate coefficients of reactions in which the mechanisms are well known, in particular, OH abstraction mechanisms. We have conducted an experimental and theoretical study of the reactions of OH with a series of alkyl sulfides in an attempt to better understand and characterize the complex behavior involved. Our goal is to develop a comprehensive predictive expression that will allow the effective rate coefficients for these reactions to be calculated under all conditions of atmospheric pressure, temperature, and composition on the basis of measurements of the rate coefficients of the fundamental elementary reactions with additional confirmation from structural additivity relationships. The practical utility of such an expression is mostly limited to the reaction of OH with dimethyl sulfide (DMS, $(CH_3)_2S$). DMS is the predominant natural source of sulfur in the atmosphere and it is the precursor of the methane sulfonate and natural fraction of the non-sea-salt sulfate (nss-$SO_4$) aerosol that is ubiquitous throughout the marine boundary layer. The importance of DMS as a source of cloud condensation nuclei has led to intense interest in understanding the rates and mechanism of the OH-initiated oxidation of DMS.[4−15] Both experimental and theoretical studies of the reaction of OH with DMS are consistent with the reaction proceeding via a two-channel mechanism involving both abstraction and addition channels. The adduct that is formed by the addition channel can react with molecular oxygen, $O_2$, or decompose back to reactants.

$$CH_3SCH_3 + OH \rightarrow \text{products} \quad (1)$$

$$CH_3SCH_3 + OH \rightarrow CH_3SCH_2 + H_2O \quad (1a)$$

$$CH_3SCH_3 + OH + M \rightarrow CH_3S(OH)CH_3 + M \quad (1f,1r)$$

$$CH_3S(OH)CH_3 + O_2 \rightarrow \text{products} \quad (1s)$$

Because of this mechanism, the effective rate coefficient for the reaction of OH with DMS shows a complex dependence on temperature, total pressure, and the partial pressure of $O_2$. We have reported measurements on reaction 1, their deuterated

* Corresponding author. E-mail: ahynes@rsmas.miami.edu.
[†] Current address: Ames Research Center, Atmospheric Sciences Division, NASA, MS 245-5, Moffett Field, CA 94035.
[‡] Current address: Department of Chemistry, University of British Columbia, Vancouver, British Columbia, Canada V6T 1Z1.

10.1021/jp9010668 CCC: $40.75 
Published on Web 05/27/2009

analogue, reaction 2, and the reactions of OH with methylethyl and diethyl sulfides, reactions 3 and 4.[5,6,16−18]

$$CD_3SCD_3 + OH \rightarrow \text{products} \quad (2)$$

$$CH_3SCH_2CH_3 + OH \rightarrow \text{products} \quad (3)$$

$$C_2H_5SC_2H_5 + OH \rightarrow \text{products} \quad (4)$$

In each case, we were able to observe the formation of the OH−alkyl sulfide adduct (RS(OH)R) directly, determine the $O_2$ dependence of the rate coefficient at 200 and 600 Torr total pressure, and show that the results are completely consistent with the two-channel mechanism shown above for reaction 1. In addition, we were able to derive values of the elementary rate coefficients for abstraction ($k_{2a}$, $k_{3a}$, $k_{4a}$), adduct formation ($k_{2f}$, $k_{3f}$, $k_{4f}$), adduct decomposition ($k_{2r,}$ $k_{3r}$, $k_{4r}$), and adduct reaction with $O_2$ ($k_{2s}$, $k_{3s,}$ $k_{4s}$). By examining the trends in the reactivity of OH with a series of alkyl sulfides, we hope to increase our confidence in our understanding of the overall mechanism and the accuracy of the rate coefficients for the elementary steps. In addition, we can examine the ability of theory to characterize the two center−three electron bond between the sulfur and oxygen atoms with changing alkyl substituents.

DPS and DBS do not have natural sources to the atmosphere, and significant anthropogenic sources have not been identified.

$$C_3H_7SC_3H_7 + OH \rightarrow \text{products} \quad (5)$$

$$C_4H_9SC_4H_9 + OH \rightarrow \text{products} \quad (6)$$

Rate coefficients for the reaction of OH radicals with DPS have been reported in two studies.[19,20] A relative rate technique was employed in the study of Barnes at al.[19] that obtained a room-temperature rate coefficient for reaction 5 of $(1.90 \pm 0.20) \times 10^{-11}$ cm$^3$·molec$^{-1}$·s$^{-1}$ under 760 Torr of $N_2$. Nielsen et al.[20] reported a room-temperature rate coefficient for the same reaction of $(2.15 \pm 0.30) \times 10^{-11}$ cm$^3$·molec$^{-1}$·s$^{-1}$ under 760 Torr of argon as well as the sole prior measurement of reaction 6, $k_{298} = (3.74 \pm 0.50) \times 10^{-11}$ cm$^3$·molec$^{-1}$·s$^{-1}$. No prior measurements of reactions 5 or 6 have been performed as a function of pressure, temperature, and oxygen concentration.

As in our prior studies of reactions 1−4, we have performed electronic structure calculations on the DPSOH and DBSOH adducts using Gaussian 03 to complement the experimental studies. On the basis of this systematic experimental and theoretical study, we examine the reactivity trends across the series of alkyl sulfides reported in this and two earlier publications.[17,18] To complete this analysis, we present additional data sets for the $O_2$ dependence of the reactions of DMS and DMS-$d_6$ with the OH radical, reaction 1 and 2. The $O_2$ dependence of the effective rate coefficient for reaction 1 at 200 and 600 Torr total pressure at ∼296 and ∼261 K and for reaction 2 at 200 and 600 Torr total pressure at ∼296 and ∼261 K are presented. Finally, we develop an expression for the effective rate coefficient for the reaction of OH with DMS, which is appropriate for all pressures, temperatures, and $O_2$ partial pressures encountered in the troposphere. This expression allows both the effective rate coefficient and the branching ratio to be calculated from elementary rate coefficients rather than an empirical fit to a limited data set.

## Experimental Section

The experimental configuration for the pulsed laser photolysis−pulsed laser-induced fluorescence system (PLP-PLIF) used in this laboratory has been described in detail elsewhere.[17,21−23] The system and experimental design employed is similar to that used in prior studies of alkyl sulfide kinetics with slight modifications in the in situ spectrophotometric analysis of dipropyl and dibutyl sulfides. A brief description is provided below. OH radicals were produced by the 266 nm photolysis of $H_2O_2$ using the fourth harmonic output from a Nd-YAG laser; initial radical concentrations were typically ∼$1 \times 10^{12}$/cm$^3$. A Nd-YAG pumped, frequency doubled, tunable dye laser was used to excite the $Q_1$1 line of the OH A-X(1−0) transition at 282 nm. Fluorescence was detected in the 0−0 and 1−1 bands with a photomultiplier tube after passing through collection optics and filters, discriminating against Rayleigh and Raman scattering from $N_2$, $O_2$, or both. The reaction vessel was a thermostatted, pyrex cell. Beams were combined with a dichroic mirror and propagated through a side arm perpendicular to both the photomultiplier tube and the direction of gas flow. The photomultiplier output was amplified and processed by a 500 MHz digital oscilloscope to obtain the area of the fluorescence signal, averaged for 50 laser shots. A digital delay generator was used to vary the time delay between the photolysis and probe beams, and signal was collected for 20−50 delays to map out the OH temporal profile. A linear flow rate of between 5 and 10 cm/s through the reaction zone was maintained to ensure no accumulation of reaction or photolysis products. Reactant concentrations were monitored in situ by photometry using either the 213.9 or 228.8 nm lines from a zinc or cadmium lamp. We have recently reported an extensive experimental study of the spectra and absolute absorption cross sections of the alkyl sulfides, and those values were used in this work.[24] Concentrations were measured simultaneously both before and after the reaction cell, and the concentration in the reaction cell was taken as the average of the two measurements. DPS and DBS concentrations were measured using the 213.9 nm line from a zinc lamp and $\sigma_{213.9} = 3.52 \times 10^{-18}$ and $4.40 \times 10^{-18}$ cm$^2$, respectively.[24] DMS and DMS-$d_6$ concentrations were measured using the 228.8 nm line from a Cadmium lamp, and $\sigma_{228.8} = 1.10 \times 10^{-18}$ and $5.07 \times 10^{-19}$ cm$^2$, respectively.[24] Sulfide loss in the reaction cell ranged from 3−12 % for DPS and DBS. Oxygen concentrations were calculated from flows. Typically, [RSR] < $1 \times 10^{15}$ molec/cm$^3$ was employed to ensure that OH temporal profiles always showed single exponential behavior. The rationale for this is discussed in more detail below. The oxygen dependence of the effective rate coefficients for reaction 5 was measured at temperatures close to target temperatures of 240, 261, and 296 K at both 200 and 600 Torr total pressure ($N_2 + O_2$) as a function of the partial pressure of oxygen. Measurements of reaction 6 were performed at 261 and 296 K at both 200 and 600 Torr total pressure. Measurements for reaction 1 are reported for 261 and 296 K at 200 and 600 Torr total pressure and for reaction 2 at 261 and 296 K at 200 Torr total pressure. Previous results were limited to 240 K only.

## Results

**1. Electronic Structure Calculations.** Geometry optimizations for DPS, DBS, and the OH adducts of these two species (DPSOH and DBSOH) and OH were completed at the MP2/6-31+G(2d,p) level of theory utilizing Gaussian 03.[25] The optimized structure of the dipropyl and dibutyl sulfide OH adducts are shown, respectively, in Figures 1 and 2. Relevant bond lengths and angles are listed in Table 1. Whereas no prior electronic structure calculations are available for the adduct species, the most critical structural parameter is the S−O bond length. In both cases, the bond lengths are in good agreement with our prior calculations for the S−O bond length in the dimethyl sulfide−OH adduct (2.047 Å),[17] the methyl−ethyl

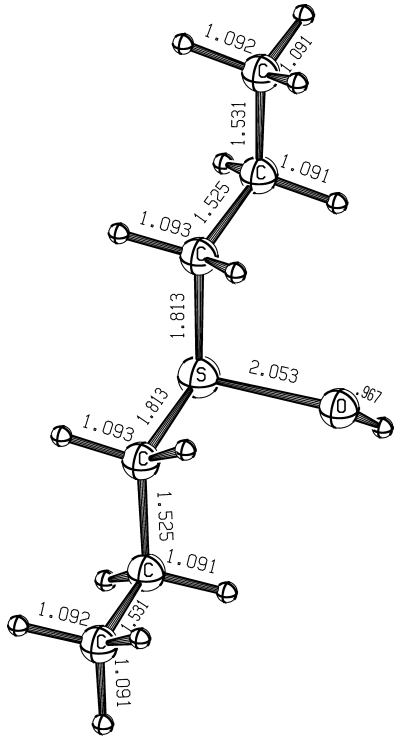


**Figure 1.** ORTEP[42] rendering of the MP2/6-31+G(2d,p) optimized structure of the dipropyl sulfide−OH adduct. Bond lengths are in angstroms. Other relevant structural parameters can be found in Table 1.

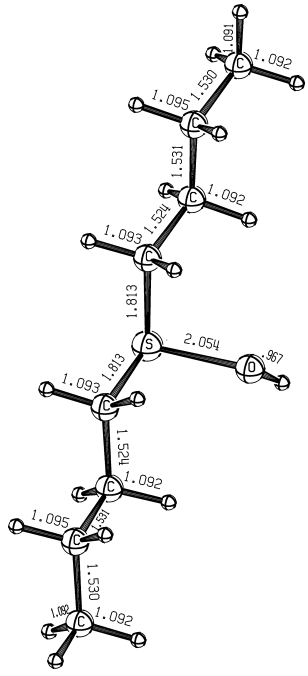


**Figure 2.** ORTEP[42] rendering of the MP2/6-31+G(2d,p) optimized structure of the dibutyl sulfide−OH adduct. Bond lengths are in angstroms. Other relevant structural parameters can be found in Table 1.

sulfide−OH adduct (2.049 Å), and the diethylsulfide−OH adduct (2.052 Å).[18]

Vibrational frequencies for all species were calculated numerically at the equilibrium geometry using the same level of theory as the geometry optimization. All of the calculated frequencies were positive, indicating that the equilibrium structures were at a minimum on the potential energy surface. In addition, zero-point energies were calculated at the MP2/6-31+G(2d,p)[26−30] level of theory for the molecules studied. The results of these calculations are found in Table 2.

Utilizing the optimized MP2/6-31+G(2d,p) geometries, we improved energies by increasing the level of the basis set to 6-311+G(3df,2p).[31] The results of these calculations are found in Table 1.

Following the method of Ochterski,[32] we calculated binding energies and enthalpies of reaction at 0, 240, 261, and 298 K for the reactions of dipropyl and dibutyl sulfide with OH using both the 6-31+G(2d,p) and 6-311+G(3df,2p) basis sets. The results of these calculations are found in Table 3.

It has generally been recognized that treating the S−O bond in this class of molecule requires utilizing electron correlation for both accurate geometries and energies. Unfortunately, because of storage and processor limitations, we were unable to treat this system with anything greater than second-order Møller−Plesset perturbation theory. However, on the basis of our work with the lower sulfide adducts, the energy for the reactions, after correction for electron correlation using the larger basis set, should lie between the two MP2 values determined at the two basis sets. Using this rationale, the DPS−OH bond strength, utilizing higher levels of electron correlation, should lie between −11.88 and −13.35 kcal/mol, and the DBS−OH bond strength should be between −12.04 and −13.52 kcal/mol. This is in good agreement with values previously reported for the DMSOH, MESOH, and DESOH adduct of −10.9, −10.13, and −11.00 kcal/mol, respectively.[17,18]

Table 4 contains a comparison of bond energies and enthalpies for the dipropyl and dibutyl sulfide adducts as well as the lower sulfides. Purely on the basis of the trend seen with the lower sulfides, one would expect the bond energies and enthalpies to increase as the size of the adduct increases. This is indeed the case with the DPS and DBS adduct species.

On the basis of these computational results, we conclude that the dipropyl sulfide−OH adduct has a bond strength of at least −11.88 kcal/mol, and the adduct forming reaction is exothermic by at least 9.83 kcal/mol at 298 K. The dibutyl sulfide−OH adduct has an even stronger bond energy of at least −12.04 kcal/mol, and the adduct forming reaction is exothermic by at least 11.29 kcal/mol at 298 K.

**2. Data Analysis.** ***2.1. Reactions 5 and 6.*** All experiments were performed under pseudo-first-order conditions with [RSR] ≫ OH. OH temporal profiles were analyzed assuming a simple exponential decay, and Figure 3 shows typical pseudo-first-order decays that were always linear over two to three orders of magnitude. Rate coefficients were obtained from plots of pseudo-first-order rate versus [RSR], and a series of typical plots are shown for reactions 5 and 6 in Figures 4 and 5. Second-order plots show good linearity, suggesting that problems associated with wall loss do not affect the precision of the measurements. In addition, it can be seen that the slopes increase with increasing partial pressure of oxygen. The oxygen dependence of the effective rate of reaction 5 was measured at total pressures of 200 and 600 Torr at 296, 261, and 240 K, and the 600 Torr results are shown in Figure 6. Similar measurements were made for reaction 6 at 298 and 261 K, and the 600 Torr results are shown in Figure 7. The low vapor pressure of DBS precluded measurements of reaction 6 at temperatures below 261 K. Data at 200 Torr is plotted in Figures S1 and S2 of the Supporting Information. The values of $k_{obs}$ obtained are tabulated, together with temperature, $O_2$ partial pressure, and total pressure, in Tables S1a and S1b of the Supporting Information.

**TABLE 1: Energies and Relevant Structural Parameters for MP2/6-31+G(2d,p) Optimized Structures of DPS, DBS, DPS−OH Adduct, DBS−OH Adduct, and OH[a]**

| molecular species | symmetry | state | energy (hartrees) MP2/6-31+G(2d,p) | energy (hartrees) MP2/6-311+G(3df,2p)[b] | structural parameter | value |
|---|---|---|---|---|---|---|
| $CH_3CH_2CH_2SCH_2CH_2CH_3$ | $C_{2v}$ | $^1A_1$ | −633.97773333173 | −634.20495891142 | C−S | 1.8246 |
| | | | | | C−S−C | 98.772 |
| $CH_3CH_2CH_2CH_2SCH_2CH_2CH_2CH_3$ | $C_{2v}$ | $^1A_1$ | −712.36114546823 | −712.64339610309 | C−S | 1.8249 |
| | | | | | C−S−C | 98.822 |
| $CH_3CH_2CH_2S(OH)CH_2CH_2CH_3$ | $C_S$ | $^2A'$ | −709.56236629789 | −709.84376092709 | C−S | 1.8128 |
| | | | | | S−O | 2.0533 |
| | | | | | O−H | 0.9666 |
| | | | | | C−S−C | 100.547 |
| | | | | | C−S−O | 87.975 |
| | | | | | S−O−H | 104.336 |
| $CH_3CH_2CH_2CH_2S(OH)CH_2CH_2CH_2CH_3$ | $C_S$ | $^2A'$ | −787.94602714145 | −788.28247439561 | C−S | 1.8130 |
| | | | | | S−O | 2.0537 |
| | | | | | O−H | 0.9666 |
| | | | | | C−S−C | 100.639 |
| | | | | | C−S−O | 87.931 |
| | | | | | S−O−H | 104.317 |
| OH | $C_{\infty v}$ | $^2\Pi$ | −75.565693601083 | −75.617531723755 | OH | 0.9703 |

[a] Bond lengths are in angstroms and bond angles are in degrees. [b] Energy calculated at MP2/6-31+G(2d,p) optimized geometry.

The analysis of the kinetic data for reactions 5 and 6 is similar to that employed in our recent studies of reactions 1−4 and assumes that the reaction proceeds via an analogous two-channel mechanism involving addition and abstraction mechanisms.

DPS:

$$C_3H_7SC_3H_7 + OH \rightarrow C_3H_7SC_3H_6 + H_2O \quad (5a)$$

$$C_3H_7SC_3H_7 + OH + M \leftrightarrow C_3H_7S(OH)C_3H_7 + M \quad (5f,5r)$$

$$C_3H_7S(OH)C_3H_7 + O_2 \rightarrow \text{products} \quad (5s)$$

DBS:

$$C_4H_9SC_4H_9 + OH \rightarrow C_4H_9SC_4H_8 + H_2O \quad (6a)$$

$$C_4H_9SC_4H_9 + OH{+}M \rightarrow C_4H_9S(OH)C_4H_9 + M$$

$$C_4H_9S(OH)C_4H_9 + M \rightarrow C_4H_9S(OH)C_4H_9 + M \quad (6f,6r)$$

$$C_4H_9S(OH)C_4H_9 + O_2 \rightarrow \text{products} \quad (6s)$$

Abstraction and addition channels are assumed to be independent, and the kinetic analysis is simplified if both pseudo-first-order conditions and the steady-state approximation as applied to the adduct are valid; that is, [RSR] ≫ [OH] ≫ [RSROH]. Applying the steady-state approximation to the adduct gives an expression, eq I, for the effective oxidation rate, $k_{obs}$, at any oxygen concentration at a fixed total pressure.

$$k_{obs} = \frac{k_a + \frac{k_s}{k_r}(k_a + k_f)[O_2]}{1 + \frac{k_s}{k_r}[O_2]} \quad (I)$$

where $k_a$ is the rate coefficient for hydrogen abstraction ($k_{5a}$ or $k_{6a}$), $k_f$ is the effective bimolecular rate coefficient for OH addition to the sulfur atom of RSR ($k_{5f}$ or $k_{6f}$) at total pressure M, $k_r$ is the effective unimolecular rate coefficient for adduct decomposition ($k_{5r}$ or $k_{6r}$) at total pressure M, and $k_s$ is the rate of adduct scavenging by $O_2$ ($k_{5s}$ or $k_{6s}$), as described in previous work.[16,17] At the lowest temperatures used in this work, $K_c \approx 1 \times 10^{-17}$ cm$^3$·molecule$^{-1}$, and hence at [RSR] < $1 \times 10^{15}$ molecules·cm$^{-3}$, the concentration of OH is at least a factor of 20 times larger than the adduct concentration, and at higher temperatures the ratio is much larger. At these relatively low concentrations of RSR, the steady-state approximation applies, and the OH decays show single exponential behavior, as shown in Figure 3. Therefore, $k_{obs}$, the effective second-order rate coefficient for reactions 5 or 6 is obtained from the variation of the pseudo-first-order decay rate, $k'$, with [RSR], as shown in Figures 4 and 5. In the absence of $O_2$, eq I reduces to $k_{obs} = k_a$, the abstraction rate coefficient. As the partial pressure of $O_2$ increases at a fixed total pressure, $k_{obs}$ increases as RS(OH)R adducts are scavenged rather than decomposing back to reactants. At higher $O_2$ and lower temperatures, the adduct may be sufficiently stable to allow every adduct to react with $O_2$ with no adducts decomposing back to reactants. Under these conditions, $k_{obs}$ "rolls off", becoming independent of $O_2$ concentration, and eq I reduces to $k_{obs} = k_a + k_f$. The magnitude of $k_f$ defines the maximum enhancement possible for $k_{obs}$ in the presence of [$O_2$], and observation of this limiting value of $k_{obs}$ gives a direct measurement of $k_f$. Consequently, we expect an initial linear variation of $k_{obs}$ with increasing $O_2$, with $k_{obs}$ eventually rolling off to an oxygen-independent value at high $O_2$. Such behavior has previously been observed in the OH-initiated oxidation of dimethyl, methyl ethyl, and diethyl sulfides (reactions 1−4). We see similar behavior for reactions 5 and 6, as shown in Figures 6 and 7 and Figures S1 and S2 of the Supporting Information, and notice nonlinear increases in the determined values of $k_f$ as alkyl substitution increases. Oxygen-dependent data at 296 K could not successfully be fit with eq I because the rate of forward addition is not well-defined at warm temperatures where the overall rate of oxidation is dominated by the abstraction channel.

*2.1.a. Rate of Hydrogen Abstraction from DPS and DBS.* From eq I, we find that in the absence of $O_2$, $k_{obs} = k_a$, which we identify as the abstraction rate coefficient. These rate coefficients for reactions 5a and 6a are compared with literature values in Table 5. Reactions 5a and 6a show no dependence on pressure and a slight negative temperature dependence within the precision of the measurements. H-atom abstractions from DMS, DMS-$d_6$, MES, and DES all show a positive temperature dependence. The value we obtain at room temperature for reaction 5a agrees with the value reported by Nielsen et al.[20] of $(1.90 \pm 0.20) \times 10^{-11}$ cm$^3$·molecule$^{-1}$·s$^{-1}$ but is slightly lower than that of Barnes et al.[19] of $(2.15 \pm 0.30) \times 10^{-11}$

**TABLE 2: Unscaled Vibrational Frequencies ($cm^{-1}$) and Zero-Point Energies ($J \cdot mol^{-1}$) Calculated at the Optimized MP2/6-31+G(2d,p) Geometry**

| molecular species | frequencies | zero-point energy |
|---|---|---|
| $CH_3CH_2CH_2SCH_2CH_2CH_3$ | 42.1846, 55.7046, 78.8205, 102.2364, 116.4235, 228.2068, 248.6729, 248.7984, 280.2719, 343.8068, 394.5103, 755.5325, 761.6596, 775.0715, 791.015, 870.0864, 884.4758, 920.8487, 926.7196,1066.6939, 1067.8946, 1068.8233,1083.0886, 1108.2843, 1139.7689, 1253.7077, 1255.7577, 1255.9960, 1283.3784, 1329.1549, 1330.2630, 1373.0874, 1383.0623, 1434.7189, 1435.0186, 1508.5877, 1515.5914, 1528.2909, 1528.4226, 1534.3011, 1534.3037, 1540.4997, 1540.7157, 3088.7878, 3091.1853, 3096.6728, 3096.9265, 3106.8779, 3107.2793, 3141.9846, 3145.5155, 3161.7001, 3164.9323, 3188.4547, 3188.7209, 3189.9009, 3189.9510 | −634.20495891142 |
| $CH_3CH_2CH_2CH_2SCH_2CH_2CH_2CH_3$ | 25.3790, 38.3402, 51.9188, 89.2564, 90.1466, 117.3855, 120.9600, 149.7324, 205.0064, 253.7076, 254.1053, 271.8384, 367.0783, 391.3572, 443.8214, 746.5553, 748.4070, 784.2607, 788.0188, 795.5465, 806.0889, 912.6507, 922.0763, 928.0510, 939.4365, 1040.0716, 1048.1844, 1076.7464, 1087.1519, 1090.0804, 1090.8991, 1121.5825, 1142.2449, 1239.3083, 1240.9767, 1241.0232, 1263.9220, 1310.5290, 1313.2815, 1333.1313, 1338.0644, 1338.1258, 1346.2791, 1396.1651, 1399.0149, 1435.8575, 1435.9922, 1508.1263, 1514.6049, 1520.5290, 1520.9676, 1529.7533, 1529.9759, 1534.9298, 1534.9433, 1541.9037, 1541.9578, 3086.5093, 3086.6846, 3088.0618, 3089.8590, 3095.9635, 3096.0550, 3097.2819, 3098.1623, 3130.0527, 3130.1602, 3142.5332, 3145.2121, 3160.5127, 3164.6263, 3186.2179, 3186.2251, 3188.0783, 3188.1172 | −712.64339610309 |
| $CH_3CH_2CH_2S(OH)CH_2CH_2CH_3$ | 53.8969, 76.8238, 78.0904, 85.5163, 97.4642, 144.4809, 222.6585, 247.4680, 250.5199, 271.8815, 281.7950, 306.3954, 348.6541, 405.7693, 498.3225, 750.7903, 760.0296, 770.2317, 784.2510, 811.3400, 864.2480, 879.2147, 922.3418, 929.6123, 1066.2309, 1068.6265, 1076.3632, 1094.2941, 1111.9487, 1142.4734, 1257.3248, 1262.4932, 1263.2202, 1287.1280, 1333.8963, 1337.9526, 1374.1892, 1384.3597, 1435.3938, 1435.7270, 1475.6735, 1484.9103, 1527.5223, 1527.8796, 1535.3488, 1535.3831, 1538.9019, 1539.1801, 3097.9062, 3098.0943, 3103.3051, 3103.4874, 3109.1752, 3109.4136, 3167.4044, 3167.5341, 3184.9291, 3185.9327, 3193.0970, 3193.3570, 3195.5715, 3196.2671, 3835.9811 | −709.84376092709 |
| $CH_3CH_2CH_2CH_2S(OH)CH_2CH_2CH_2CH_3$ | 32.0349, 50.3036, 56.5750, 76.0318, 82.6865, 118.3971, 129.3929, 142.2923, 151.4120, 202.0950, 247.6320, 254.5779, 262.0608, 294.3671, 299.0607, 382.1435, 391.5009, 442.2853, 499.2157, 746.2132, 750.3338, 778.6612, 782.0892, 788.1318, 797.8351, 813.7053, 913.7518, 922.1438, 926.6781, 937.5413, 1040.8037, 1050.1827, 1085.8738, 1088.1091, 1090.8741, 1103.1536, 1123.5591, 1143.6188, 1242.0325, 1246.0878, 1246.6294, 1267.0092, 1315.4354, 1321.1552, 1336.2742, 1343.0060, 1343.7381, 1349.3779, 1397.0607, 1399.9318, 1436.2124, 1436.3534, 1475.2968, 1484.3178, 1520.1677, 1520.7575, 1528.2403, 1528.3235, 1535.3843, 1535.3928, 1541.2741, 1541.3211, 3087.5757, 3087.7857, 3094.3962, 3094.4632, 3097.0987, 3097.2188, 3106.6468, 3106.8744, 3137.4843, 3137.5261, 3163.7270, 3164.0269, 3186.4476, 3186.6301, 3188.7122, 3190.0643, 3190.5274, 3191.0440, 3835.7394 | −788.28247439561 |
| OH | 3817.2369 | −75.617531723755 |

$cm^3 \cdot molecule^{-1} \cdot s^{-1}$. Rate coefficients measured in our system ultimately depend on the accuracy of the UV absorption cross section. Agreement of our measurement with that of Barnes et al., which does not depend on UV cross-section measurements, suggests that the cross section used in this study is accurate. The only prior measurement of reaction 6 is at room temperature, also from Nielsen et al., and is approximately 30% faster than the value we report here, $(3.74 \pm 0.50) \times 10^{-11}$ $cm^3 \cdot molecule^{-1} \cdot s^{-1}$.

*2.1.b. Rate of OH Addition to DPS and DBS.* Figures 6 and 7 show the dependence of the effective rate coefficient on $O_2$ partial pressure for reactions 5 and 6. These are the first reported observations of an $O_2$ dependence in the rate coefficients for these reactions, and as with prior alkyl sulfides, it is clear that this dependence is absolutely consistent with a two-channel oxidation mechanism analogous to that observed in the OH/DMS system. As $O_2$ is added to the system, the contribution of the forward addition channel ($k_f$) to the overall rate is increased, resulting in the observed oxygen dependence of $k_{obs}$ in Figures 6 and 7. At low temperatures, $k_{obs}$ asymptotically approaches a limiting rate in $O_2$ where $k_{obs} = k_a + k_f$. The maximum rate enhancement in $O_2$ is well-defined when plots of $k_{obs}$ versus $[O_2]$ roll off to an $O_2$-independent region. The rate enhancement is larger, and the approach to the limiting rate is more rapid at low temperatures because of increased adduct stability. At 298 K, the $O_2$ enhancement is small compared with the magnitude of the abstraction rate coefficients and is difficult to discern at the precision of these measurements.

**TABLE 3: Comparison of Energies and Enthalpies of Reaction As a Function of Temperature and Basis Set[a]**

| | $C_3H_7SC_3H_7 + OH \rightarrow C_3H_7S(OH)C_3H_7$ | | | | |
|---|---|---|---|---|---|
| method | $\Delta E$ | $\Delta H^{0K}$ | $\Delta H^{240K}$ | $\Delta H^{261K}$ | $\Delta H^{298K}$ |
| MP2/6-31+G(2d,p) | −11.88 | −8.96 | −9.83 | −9.84 | −9.83 |
| MP2/6-311_G(3df,2p) | −13.35 | −10.42 | −11.30 | −11.30 | −11.29 |
| | $C_4H_9SC_4H_9 + OH \rightarrow C_4H_9S(OH)C_4H_9$ | | | | |
| MP2/6-31+G(2d,p) | −12.04 | −9.08 | −9.97 | −9.97 | −9.96 |
| MP2/6-311_G(3df,2p) | −13.52 | −10.56 | −11.45 | −11.45 | −11.44 |

[a] In all cases, the zero-point energy and enthalpy corrections were computed at the MP2/6-31+G(2d,p) level of theory. [b] No recommended frequency scaling factor exists in the literature for the combination of MP2 with the 6-31+G(2d,p) basis set. 0.9392 is the recommended factor for MP2/6-31+G(d,p) enthalpy calculations (CCCBDB vibrational frequency scaling factors, http://srdata.nist.gov/cccbdb/csf.asp) and was used because of the similarity to the basis set used for the calculations.

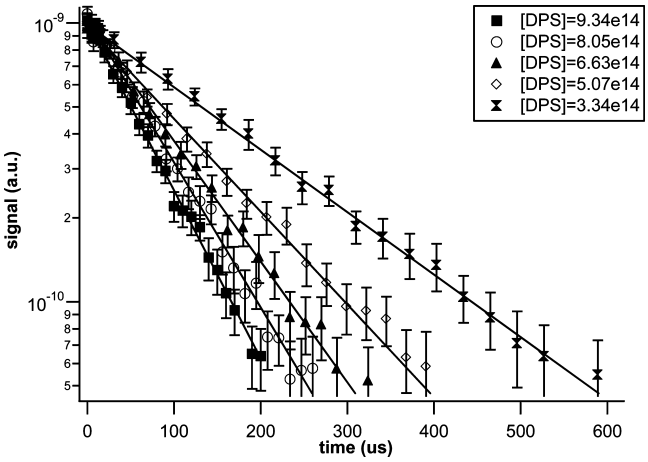


**Figure 3.** Typical OH decays in the presence of excess [DPS] at a total pressure of 200 Torr ($N_2 + O_2$), $O_2$ partial pressure of 20 Torr, and 261 K.

As in previous work, a variant of eq I was used to fit the oxygen-dependent data. In this approach, $k_r$ does not appear explicitly in eq I but is replaced by $K_c/k_f$ (eq II).

$$k_{obs} = \frac{k_a + \frac{K_c k_s}{k_f}(k_a + k_f)[O_2]}{1 + \frac{K_c k_s}{k_f}[O_2]} \qquad \text{(II)}$$

At high [RSR], the steady-state approximation breaks down as [OH] and [RS(OH)R] become comparable, and under some conditions, direct observation of equilibration and an experimental determination of $k_f$ and $k_r$ and hence $K_c$ is possible. We have made such observations for lower alkyl sulfides at low temperature, but this was not possible for DPS and DBS. As in our prior work on methyl ethyl sulfide (MES) and diethyl sulfide (DES), the data were fit with $K_c$ as a fixed parameter using values determined from the van't Hoff parameters for DMSOH adduct formation.[17] The theoretical calculations described above support this approach because the structures of all of the OH−alkyl sulfide adducts are very similar, and the calculated entropy and enthalpy changes associated with adduct formation are very similar in each case. The abstraction rate measured during the experiment was also fixed, leaving only $k_f$ and $k_s$ as free parameters with $k_{obs}$ and $[O_2]$ as the measured quantities.

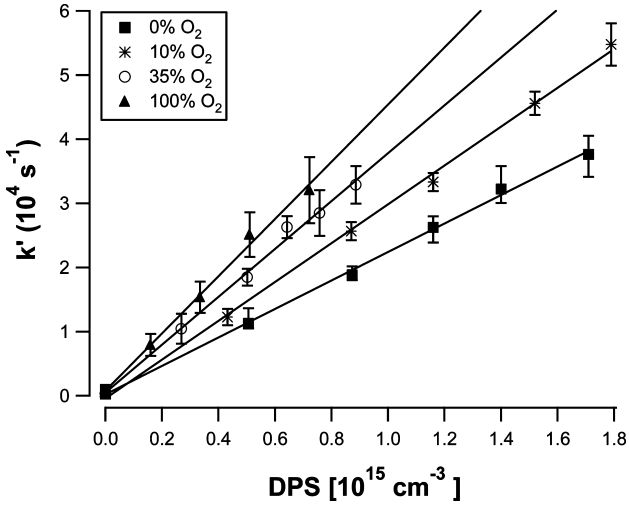


**Figure 4.** Pseudo-first-order decay rates ($k'$) plotted as a function of [DPS] at various partial pressures of $O_2$. Total pressure ($N_2 + O_2$) = 200 Torr and temperature = 261 K. Overall rate of reaction 5 increases with increasing partial pressure of $O_2$.

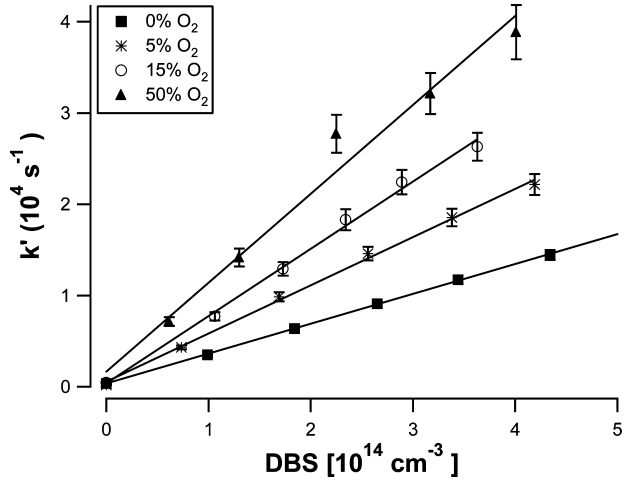


**Figure 5.** Pseudo-first-order decay rates ($k'$) plotted as a function of [DBS] at various partial pressures of $O_2$. Total pressure ($N_2 + O_2$) = 200 Torr and temperature = 261 K. Overall rate of reaction 6 increases with increasing partial pressure of $O_2$.

**TABLE 4: Comparison of Calculated Reaction Energies (kcal/mol)**

| | MP2/6-31+G(2d,p) | | | MP2/6-311+G(3df,2p) | | |
|---|---|---|---|---|---|---|
| species | $\Delta E$ | $\Delta H^{0K}$ | $\Delta H^{298K}$ | $\Delta E$ | $\Delta H^{0K}$ | $\Delta H^{298K}$ |
| DMS−OH[1] | −9.50 | −6.85 | −7.57 | −11.16 | −8.51 | −9.22 |
| MES−OH[2] | −10.55 | −7.78 | −8.59 | −12.11 | −9.33 | −10.14 |
| DES−OH[2] | −11.54 | −8.67 | −9.54 | −13.06 | −10.19 | −11.06 |
| DPS−OH | −11.88 | −8.96 | −9.83 | −13.35 | −10.42 | −11.29 |
| DBS−OH | −12.04 | −9.08 | −11.29 | −13.52 | −10.56 | −11.44 |

[a] Reference 17. [b] Reference 18.

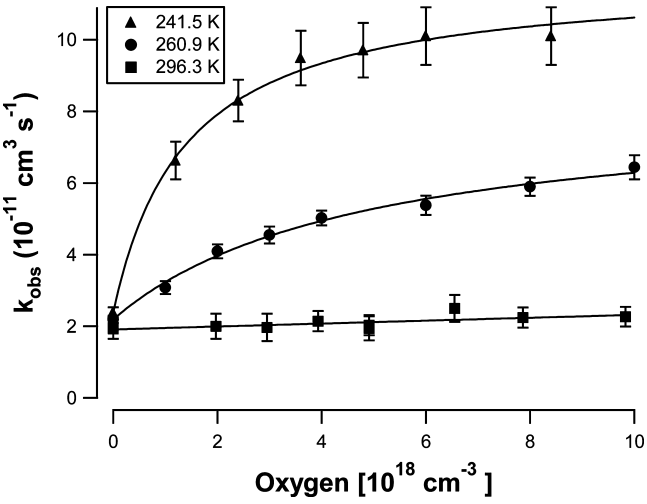


**Figure 6.** Effective rate of reaction 5 plotted as a function of oxygen partial pressure and a total pressure of ($N_2 + O_2$) of 600 Torr and three different temperatures (241.5, 260.9, 296.3 K). The contribution of the forward addition channel ($k_{5f}$) increases at colder temperatures and higher partial pressures of oxygen because of increased adduct stability.

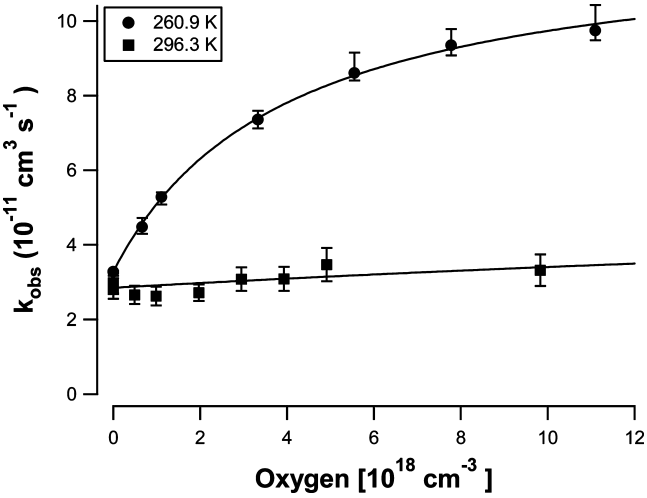


**Figure 7.** Effective rate of reaction 6 plotted as a function of oxygen partial pressure and a total pressure of ($N_2 + O_2$) of 600 Torr and two different temperatures (260.9 and 296.3 K). The contribution of the forward addition channel ($k_{6f}$) increases at colder temperatures and higher partial pressures of oxygen because of increased adduct stability.

**TABLE 5: Comparison of Abstraction Rate Coefficients**

| reaction | $T$ (K) | $k_a \times 10^{-11}$ (cm$^3$·molecule$^{-1}$·s$^{-1}$) | ref |
|---|---|---|---|
| DPS+OH | 298 | 1.92 ± 0.06 | this work |
| | 261 | 2.20 ± 0.07 | |
| | 240 | 2.55 ± 0.56 | |
| | 295 | 2.15 ± 0.30 | Barnes et al.[19] |
| | 293 | 1.90 ± 0.20 | Nielsen et al.[20] |
| DBS+OH | 298 | 2.83 ± 0.28 | this work |
| | 261 | 3.43 ± 0.42 | |
| | 295 | 3.74 ± 0.50 | Nielsen et al.[20] |

The values of $k_f$ and $k_s$ that were obtained when we fit the oxygen dependence of reactions 5 and 6 data are shown in Table 6. In addition, we obtained fits by allowing $K_c$, $k_f$, and $k_s$ to vary freely, and the results were very similar to those obtained with the constrained $K_c$. The solid lines in Figures 6 and 7 and Figures S1 and S2 in the Supporting Information show the calculated $O_2$ dependence of $k_{obs}$ for reactions 5 and 6 using the values of $k_f$ and $k_s$ obtained from the fits. This approach gives values of $k_s$ that range between (0.6 and 4) × $10^{-12}$ cm$^3$·molecule$^{-1}$·s$^{-1}$ for all sulfides studied. However, as we discuss below, these values are calculated using the van't Hoff expression for DMS. The results suggest, within the precision of our measurements, that RSROH adduct scavenging by $O_2$ does not have a significant temperature or pressure dependence. It should be noted that $K_c$ and $k_s$ are inverse parameters in the fit and cannot be decoupled, however the value of $k_f$ is well defined by the "rolloff" in $k_{obs}$.

As in our previous work, we fit the rate coefficients for pressure-dependent three-body recombination reactions using the formalism of Troe.[33]

$$k = \frac{k_0[\mathrm{M}]}{1 + k_0[\mathrm{M}]/k_\infty} F_c \left[1 + \left(\frac{\log(k_0[\mathrm{M}]/k_\infty)}{N}\right)^2\right]^{-1}$$
$$N = (0.75 - 1.27)\log(F_c) \qquad \text{(III)}$$

Because we only have two data points in each set (200 and 600 Torr), there are multiple solutions. However, taking the physically realistic requirement that $F_c \leq 1$, we find that the data for DPS at 240 K are close to the high-pressure limit, and $k_\infty$ does not strongly depend on the fit value of $F_c$. For $F_c = 1$, we obtain $k_\infty = 1.10 \times 10^{-10}$ cm$^3$·molecule$^{-1}$·s$^{-1}$, and with $F_c = 0.6$, we obtain $k_\infty = 1.27 \times 10^{-10}$ cm$^3$·molecule$^{-1}$·s$^{-1}$. For DBS, it was not possible to obtain data at 240 K; a similar analysis of the 261 K data gives a value of $k_\infty = 1.9 \times 10^{-10}$ cm$^3$·molecule$^{-1}$·s$^{-1}$ using $F_c = 1$ and $k_\infty = 4.4 \times 10^{-10}$ cm$^3$·molecule$^{-1}$·s$^{-1}$ with $F_c = 0.6$. We discuss these values further and provide graphic representations in our examination of reactivity trends below.

***2.2. Reaction 1 and 2.*** In a previous work, we reported a low-temperature study of reaction 1 and 2 that included direct observations of the pressure dependence of adduct formation together with a study of the $O_2$ dependence of the effective rate coefficients for reaction 1 and 2.[17] We extracted elementary rate coefficients and developed an expression for the effective rate coefficient of reaction 1 at low temperature. In this work, we report additional data sets for reaction 1 and 2 that allow us to extend this analysis over the temperature range of 240−300 K and compare the results with those of reactions 3−6. The data sets that give the $O_2$ dependence of reaction 1 and 2 at 200 and 600 Torr total pressure at 296 and 261 K are listed in Tables S2a and S2b of the Supporting Information. The results for reaction 2 at 600 Torr and 240 K have been presented in graphical form in a prior publication.[6] The data was analyzed using eq II with $K_c$ being taken from the van't Hoff expression reported in a prior work. The values of the abstraction rate coefficients were fixed at the value measured in the absence of $O_2$. Values of the forward coefficients ($k_f$), adduct decomposition rate coefficients ($k_r$) $k_{1r}$ and $k_{2r}$, and the rate coefficients for the adduct reaction with $O_2$ ($k_s$), $k_{1s}$ and $k_{2s}$, are listed in Table 7. The 240 K rate coefficients for Reactions 1 and 2 as well as the rate coefficients obtained for reactions 3 and 4 obtained in our previous works are shown together with coefficients obtained in this work for easy comparison in Table S3 of the Supporting Information. Figure 8 shows the $O_2$ dependence of the effective rate coefficients for Reactions 1 and 2 at 600 Torr total pressure and 296 or 261 K. The lines show the calculated dependence using the rate coefficients in Table 7. We again find that the data can be fit assuming a simple two-channel mechanism and using a common van't Hoff expression determined for the formation of DMSOH adduct. The value of $k_s$, (7 ± 2) × $10^{-13}$ cm$^3$·molecule$^{-1}$·s$^{-1}$, is similar for both

**TABLE 6: Fits of Equation II to $O_2$-Dependent Data for Reactions 5 and 6**

| | $P$ (Torr) | $T$ (K) | $K_c$ fixed | $k_a$ ($cm^3 \cdot molec^{-1} \cdot s^{-1}$) fixed | $k_f$ ($cm^3 \cdot molec^{-1} \cdot s^{-1}$) free | $k_s$ ($cm^3 \cdot molec^{-1} \cdot s^{-1}$) free |
|---|---|---|---|---|---|---|
| DPS+OH | 600 | 296.3 | $7.43 \times 10^{-19}$ | $1.93 \times 10^{-11}$ | $(2.03 \pm 700) \times 10^{-10}$ | $(5.67 \pm 40) \times 10^{-13}$ |
| DPS+OH | 600 | 260.9 | $8.06 \times 10^{-18}$ | $2.19 \times 10^{-11}$ | $(6.07 \pm 2.14) \times 10^{-11}$ | $(1.33 \pm 0.50) \times 10^{-12}$ |
| DPS+OH | 600 | 241.6 | $4.01 \times 10^{-17}$ | $2.38 \times 10^{-11}$ | $(9.39 \pm 3.30) \times 10^{-11}$ | $(1.68 \pm 1.41) \times 10^{-12}$ |
| DPS+OH | 200 | 297.1 | $7.09 \times 10^{-19}$ | $1.91 \times 10^{-11}$ | | |
| DPS+OH | 200 | 261.1 | $7.94 \times 10^{-18}$ | $2.16 \times 10^{-11}$ | $(2.87 \pm 0.5) \times 10^{-11}$ | $(1.75 \pm 0.46) \times 10^{-12}$ |
| DPS+OH | 200 | 240.3 | $4.50 \times 10^{-17}$ | $2.77 \times 10^{-11}$ | $(7.04 \pm 0.38) \times 10^{-11}$ | $(1.06 \pm 0.09) \times 10^{-12}$ |
| DBS+OH | 600 | 296.3 | $7.56 \times 10^{-19}$ | $2.91 \times 10^{-11}$ | $(3.54 \pm 63) \times 10^{-11}$ | $(8.74 \pm 27) \times 10^{-13}$ |
| DBS+OH | 600 | 260.9 | $8.06 \times 10^{-18}$ | $3.28 \times 10^{-11}$ | $(9.01 \pm 2.91) \times 10^{-11}$ | $(2.86 \pm 0.81) \times 10^{-12}$ |
| DBS+OH | 200 | 296.4 | $7.38 \times 10^{-19}$ | $2.78 \times 10^{-11}$ | | |
| DBS+OH | 200 | 261.3 | $7.82 \times 10^{-18}$ | $3.58 \times 10^{-11}$ | $(3.84 \pm 0.48) \times 10^{-11}$ | $(3.10 \pm 0.64) \times 10^{-12}$ |

**TABLE 7: Fits of Equation II to $O_2$-Dependent Data for Reactions 1−1s and 2**

| | $P$ (Torr) | $T$ (K) | $K_c$ fixed | $k_a$ ($cm^3 \cdot molec^{-1} \cdot s^{-1}$) fixed | $k_f$ ($cm^3 \cdot molec^{-1} \cdot s^{-1}$) free | $k_s$ ($cm^3 \cdot molec^{-1} \cdot s^{-1}$) free |
|---|---|---|---|---|---|---|
| DMS-$h_6$+OH | 600 | 296.8 | $7.21 \times 10^{-19}$ | $4.22 \times 10^{-12}$ | $(5.82 \pm 7.42) \times 10^{-12}$ | $(7.13 \pm 4.50) \times 10^{-13}$ |
| DMS-$h_6$+OH | 600 | 260.5 | $8.32 \times 10^{-18}$ | $3.93 \times 10^{-12}$ | $(1.32 \pm 0.12) \times 10^{-11}$ | $(7.27 \pm 1.12) \times 10^{-13}$ |
| DMS-$h_6$+OH | 200 | 296.5 | $7.34 \times 10^{-19}$ | $4.05 \times 10^{-12}$ | $(1.77 \pm 0.89) \times 10^{-12}$ | $(7.54 \pm 3.26) \times 10^{-13}$ |
| DMS-$h_6$+OH | 200 | 261.4 | $7.76 \times 10^{-18}$ | $3.92 \times 10^{-12}$ | $(5.00 \pm 0.26) \times 10^{-12}$ | $(6.71 \pm 0.41) \times 10^{-13}$ |
| DMS-$d_6$+OH | 600 | 295.4 | $7.84 \times 10^{-19}$ | $1.87 \times 10^{-12}$ | $(6.07 \pm 0.58) \times 10^{-12}$ | $(7.72 \pm 0.60) \times 10^{-13}$ |
| DMS-$d_6$+OH | 600 | 261.1 | $7.94 \times 10^{-18}$ | $1.58 \times 10^{-12}$ | $(2.24 \pm 0.34) \times 10^{-11}$ | $(8.32 \pm 1.20) \times 10^{-13}$ |
| DMS-$d_6$+OH | 200 | 297.5 | $6.92 \times 10^{-19}$ | $1.67 \times 10^{-12}$ | $(2.11 \pm 0.28) \times 10^{-12}$ | $(6.70 \pm 0.44) \times 10^{-13}$ |
| DMS-$d_6$+OH | 200 | 261.0 | $8.00 \times 10^{-18}$ | $1.39 \times 10^{-12}$ | $(7.27 \pm 0.14) \times 10^{-12}$ | $(7.14 \pm 0.17) \times 10^{-13}$ |

reactions and consistent with the value obtained at 240 K. Again, we find a value of $k_s$ that, within the precision of our measurements, is independent of both temperature and pressure and similar to the value we obtain for the higher sulfides. The most striking difference in the two data sets is the $O_2$ enhancement in the rate coefficient at 261 K with a significantly larger enhancement for reaction 2. This is reflected in the significantly larger value of the forward addition rate coefficient for reaction 2. In prior work, we have always assumed that the addition channel shows no isotopic dependence; indeed, the fact that the $O_2$ enhancement showed no isotopic dependence was a key argument in Hynes et al.[4] proposing a two-channel mechanism. In fact, all of our data suggests that the forward addition rate coefficient for reaction 2 is faster than that for reaction 1 at temperatures below 298 K. The difference between the two rate coefficients varies as a function of temperature and pressure. An analysis of the data from Hynes et al. also shows a small but consistent difference, with the $O_2$ enhancement for reaction 2 always being larger at temperatures below 298 K. It is not unreasonable that the falloff behavior of the two isotopomers should be somewhat different.

*2.2a. Abstraction Rates for DMS and DMS-$d_6$.* In the absence of $O_2$,we obtain the rate coefficients for abstraction, $k_{1a}$ and $k_{2a}$. Taking these rate coefficients, together with the data we obtained at 240 K, we can derive Arrhenius expressions for reactions $k_{1a}$ and $k_{2a}$

$$k_{1a} = 7.23 \times 10^{-12} \exp(-167/T)\ cm^3 \cdot molecule^{-1} \cdot s^{-1} \quad \text{(IV)}$$

$$k_{2a} = 5.14 \times 10^{-12} \exp(-324/T)\ cm^3 \cdot molecule^{-1} \cdot s^{-1} \quad \text{(V)}$$

Data for reaction 1 are shown together with our previous measurements in Figure 9 and are listed in Table S3 of the Supporting Information. Our measurements are consistent with the previous measurements, again showing no pressure dependence, a positive activation energy, and a significant kinetic isotope effect. The precision of these measurements is better

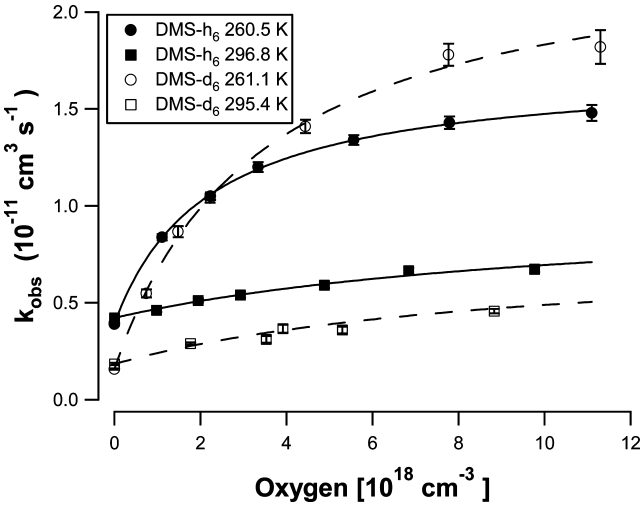


**Figure 8.** Effective rate of Reactions 1 and 2 plotted as a function of oxygen partial pressure and a total pressure of ($N_2$ + $O_2$) of 600 Torr and two different temperatures (~261 and ~296 K). Offsets in the $y$ intercept are due to differences in the H-atom abstraction rate.

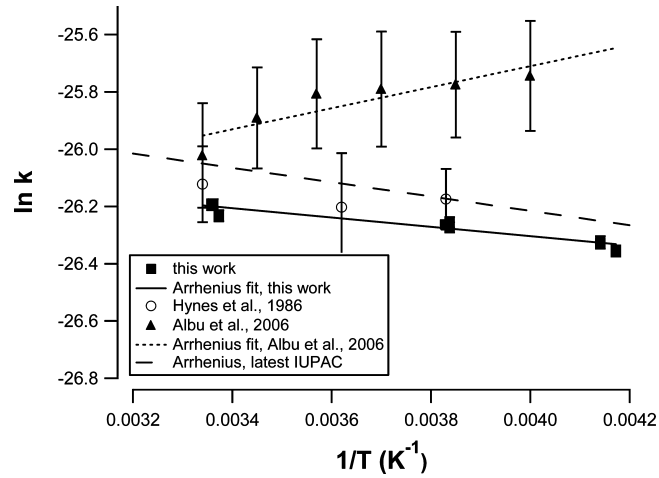


**Figure 9.** Arrhenius relationship for $k_{1a}$ as measured in this work (■), by Hynes et al.[4] (○), and by Albu et al.[8] (▲). Shown for comparison is the most recent IUPAC recommendation for temperature dependence in $k_{1a}$.

than that of our previous data; however, they lie a little below the most recent IUPAC panel Arrhenius expression[34] for reaction 1, which is shown as a dashed line in Figure 9. For comparison, we also show the recent work of Albu et al.,[8] who, in a competitive rate study, found a slight negative activation energy for reaction 1. The available data on the abstraction channel are discussed in detail in the work of Albu et al. and in the IUPAC panel recommendation. Most of the direct studies of reaction 1 find a positive activation energy for reaction, and the difference between this work and the recent work of Albu et al., which is larger than the precision associated with each measurement, is difficult to explain, particularly because the $O_2$ enhancement measured in both studies is in good agreement. In recent work, González−García and coworkers proposed that the H-atom abstraction channel proceeds via both direct and indirect channels and predicted a pressure dependence in the abstraction rate coefficient that is most pronounced at low temperatures.[15] We see no evidence of such a pressure dependence. Studies of reaction 2 might cast additional light on this, but, unfortunately, they are limited.

***2.3. Reactivity Trends in the Alkyl Sulfides.*** We have now measured the oxygen, temperature, and pressure dependence of the effective rate coefficients for a series of five reactions of alkyl sulfides with the OH radical and were able to obtain direct measurements of adduct formation for three of these reactions. We now consider the reactivity trends in the context of the two-channel oxidation mechanism.

*2.3a. Structural Additivity of Abstraction Rate Coefficients.* We have identified the oxygen-independent channel with a direct H-atom abstraction process. Stickel and coworkers measured branching ratios for the abstraction channels for an isotopomeric variant of reaction 1 and 3 measuring the HDO yields from the reactions of OD with DMS and MES at low pressure.[35] They obtained a yield of $0.85 \pm 0.15$ and suggested that whereas the results were consistent with abstraction being the major channel, the presence of a minor channel could not be excluded. A possible complication in the work of Stickel and coworkers[35] is the use of $DNO_3$ as the OD precursor. We have observed large enhancements in the observed rate coefficients for Reactions 1 and 2 in the presence of nitric acid, which suggests that nitric acid reacts more rapidly with the OHDMS adduct than with $O_2$.[36] In later work, Wine et al. measured the methyl radical yield from the reaction of OD with DMS.[37] They found that the yield of methyl radicals was negligible and suggested that, in the absence of $O_2$, reaction proceeds solely by an abstraction channel. We have analyzed our data using the "structure−activity relationships" (SAR) approach of Atkinson[1] using the values for primary and secondary abstraction rates given in that work and a value for the chemical substituent factor, $F$, $F(-S-) = 7.8$ provided in the update.[38] The substituent scaling factor, $Fx$, was not adjusted for temperature. Values of predicted rate coefficients are compared with our measured room-temperature values in Table 8. With the exception of Reactions 1 (DMS), the observed and predicted rate coefficients agree reasonably well. For reaction 1, the measured rate coefficient is two times larger. The SAR approach assumes that a substituent "activates" only the H atoms on adjacent carbon atoms, and within the precision of our measurements, the increase in reactivity with chain length is consistent with that assumption. Nielsen et al. obtained a significantly faster rate coefficient for reaction 6 (DBS) and suggested that the substituent activation extends to the H atoms on the $\beta$ and $\gamma$ C atoms. Our SAR analysis indicates that almost all of the reactivity is associated with abstraction of the $\alpha$ H atoms for all of these reactions. The contrast between the positive activation energies seen for Reactions 1 and 2 and the temperature-independent or slightly negative activation energies seen for the higher sulfides is interesting and similar to negative temperature dependencies observed over certain temperature ranges for H-atom abstraction from diethyl, dipropyl, and *n*-dibutyl ethers.[39] A study of the kinetic isotope effects for these reactions would be valuable.

**TABLE 8: Comparison of H-Atom Abstraction Rates Measured in This Laboratory at 600 Torr ($k_{obs}$) (Refs 17 and 18 and this work) with H-Atom Abstraction Rates Calculated ($k_{predict}$) Using the Structure−Activity Relationship (SAR) Method of Atkinson et al.[1] and Kwok et al.[38]**

| reaction | $T$ (K) | $k_{obs} \times 10^{-12}$ ($cm^3 \cdot molec^{-1} \cdot s^{-1}$) | $k_{predict} \times 10^{-12}$ ($cm^3 \cdot molec^{-1} \cdot s^{-1}$) |
|---|---|---|---|
| R1. $(CH_3)_2S + OH \rightarrow CH_3SCH_2 + H_20$ | 296.8 | $(4.22 \pm 0.07)$ | 2.21 |
| | 260.5 | $(3.93 \pm 0.07)$ | 1.48 |
| | 240.6 | $(3.84 \pm 0.08)$ | 1.15 |
| R3. $CH_3SC_2H_5 + OH \rightarrow CH_3SC_2H_4 + H_20$ | 296.0 | $(7.84 \pm 0.62)$ | 7.77 |
| | 261.0 | $(8.20 \pm 0.64)$ | 6.47 |
| | 242.0 | $(8.22 \pm 0.70)$ | 5.85 |
| R4. $(C_2H_5)_2S + OH \rightarrow C_2H_5SC_2H_4 + H_20$ | 296.0 | $(18.1 \pm 0.90)$ | 13.3 |
| | 260.5 | $(19.6 \pm 0.70)$ | 11.4 |
| | 241.8 | $(16.5 \pm 0.60)$ | 10.5 |
| R5. $(C_3H_7)_2S + OH \rightarrow C_3H_7SC_3H_6 + H_20$ | 296.3 | $(19.3 \pm 2.80)$ | 19.3 |
| | 260.9 | $(21.9 \pm 10.0)$ | 16.6 |
| | 241.6 | $(23.8 \pm 15.0)$ | 15.2 |
| R6. $(C_3H_9)_2S + OH \rightarrow C_4H_9SC_4H_8 + H_20$ | 296.0 | $(29.1 \pm 3.50)$ | 22.0 |
| | 261.1 | $(32.8 \pm 3.00)$ | 19.0 |

*2.3b. Structural Additivity of the Addition Channel.* Our observations of the reactivity pattern of the addition channel are qualitatively consistent with expectations. Figures 10 and 11 show the $O_2$ enhancements at 261 and 240 K at 600 Torr total pressure. We see a trend in which the $O_2$ enhancement increases with increasing length of the alkyl side chains. Interestingly, the increase in the $O_2$ enhancement that we expect to see with increasing molecular complexity does not show a simple dependence on the number of carbon atoms. At 261 K, DMS shows the smallest enhancement, DMS-$d_6$ and MES are similar, and then we see a significant increase for reactions 4,

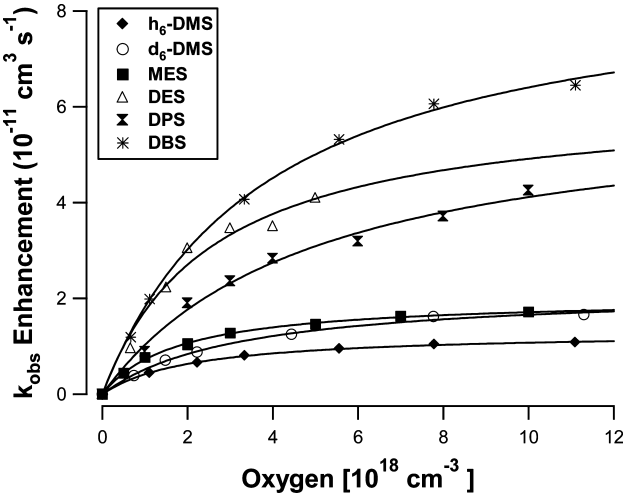


**Figure 10.** Enhancement ($k_{obs} - k_a$) in the effective rate of oxidation for all sulfides measured in this work (reactions 1−6) as a function of partial pressure of oxygen, 600 Torr total pressure ($N_2 + O_2$), and T ≅ 261 K. The enhancement increases with increasing alkyl substitution on the S atom.

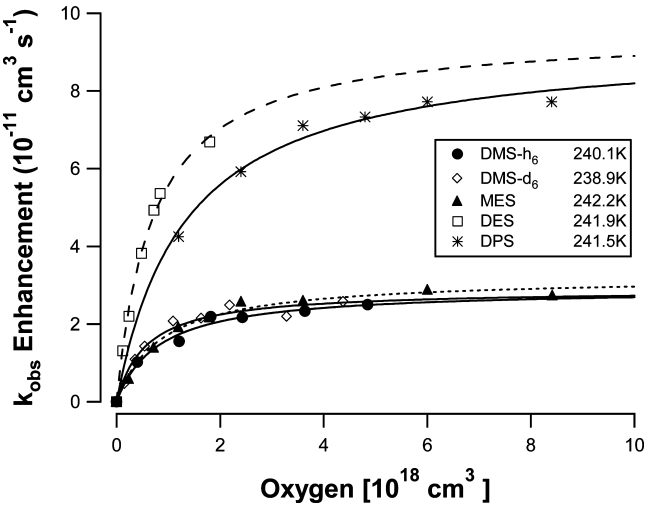


**Figure 11.** Enhancement ($k_{obs} - k_a$) in the effective rate of oxidation for reactions 1−5 as a function of partial pressure of oxygen, 600 Torr total pressure ($N_2 + O_2$), and T ≅ 240K. The enhancement increases with increasing alkyl substitution on the S atom. Because of the low vapor pressure of DBS, it was not possible to measure reaction 6 as a function of oxygen at temperatures below 261 K.

**TABLE 9: Falloff Parameters for Adduct Formation**

| sulfide | $T$ | $k_0$ ($cm^6 \cdot molec^{-2} \cdot s^{-1}$) | $k_\infty$ ($cm^3 \cdot molec^{-1} \cdot s^{-1}$) |
|---|---|---|---|
| $h_6$-DMS | 240 | $1.7 \times 10^{-30}$ | $9.4 \times 10^{-11}$ |
| | 242 | $1.7 \times 10^{-30}$ | $6.5 \times 10^{-11}$ |
| | 245 | $1.9 \times 10^{-30}$ | $3.5 \times 10^{-11}$ |
| | 261 | $6.6 \times 10^{-31}$ | $7.7 \times 10^{-11}$ |
| $d_6$-DMS | 239−241 | $2.3 \times 10^{-30}$ | $8.4 \times 10^{-11}$ |
| | 245 | $2.1 \times 10^{-30}$ | $4.3 \times 10^{-11}$ |
| | 261 | | |
| MES | 241.0 | $2.9 \times 10^{-30}$ | $8.1 \times 10^{-11}$ |
| | 261.0 | $1.2 \times 10^{-30}$ | $7.5 \times 10^{-11}$ |
| DES | 240 | $1.2 \times 10^{-29}$ | $1.5 \times 10^{-10}$ |
| | 260.5 | $6.5 \times 10^{-30}$ | $1.1 \times 10^{-10}$ |
| DPS | 240.9 | $2.4 \times 10^{-29}$ | $1.1 \times 10^{-10}$ |
| | 261 | $5.7 \times 10^{-30}$ | $1.3 \times 10^{-10}$ |
| DBS | 261 | $7.9 \times 10^{-30}$ | $1.9 \times 10^{-1}$ |

5, and 6. However, the enhancement for DES is significantly larger than for DPS with a further increase for DBS. At 240 K, we see a similar pattern, although reactions 1−3 show similar behavior, and we do not have data for DBS at 240 K. Intuitively, we might expect that MES would show a larger enhancement than DMS, and DPS would be expected to show a larger enhancement than DES.

A more quantitative analysis of the falloff behavior must be viewed with caution because of the limited amount of data. We have fit all of the data sets using the Troe formalism with a broadening factor, $F_c$, of 1, that is, the limiting case of simple Lindemann behavior, and also with the generic 0.6, as used in the NASA-JPL formulations.[40] Table 9 gives the values of $k_0$ and $k_\infty$ with a value of $F_c = 1$, which gives a lower limit to the rate coefficients for $k_0$ and $k_\infty$. For all of the data sets with the exception of the 240 K DPS data, the pressure dependence is in the linear or falloff region, and we are far from the high-pressure limit. Given the size of these molecules, this reflects the weakly bound nature of the OH−alkyl sulfide adducts. Consequently, the values of $k_0$ are relatively insensitive to the value of $F_c$, although it has a large impact on the values of $k_\infty$. Fits using $F_c = 1.0$ are shown in Figures 12 and 13, but fits with $F_c = 0.6$ are essentially indistinguishable over this pressure range. Increases in the values of $k_0$ are consistent with the increase in molecular size. The 261 K rate coefficients show

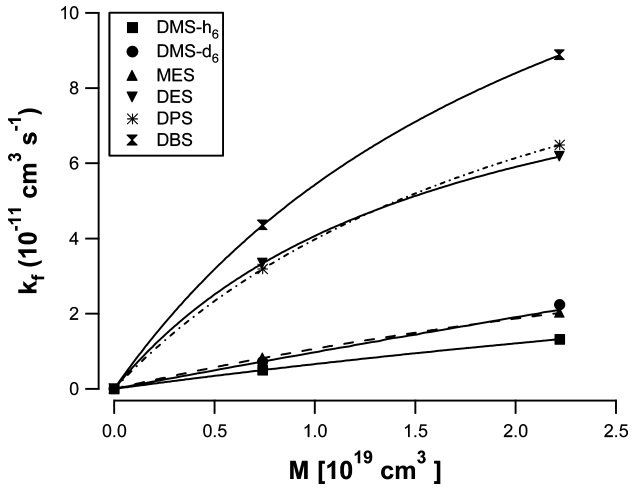


**Figure 12.** Rates of forward addition ($k_{1f-6f}$) plotted as a function of total pressure at temperatures ∼261 K. Values of $k_f$ were determined from fits of eq II to oxygen-dependent data. Solid lines are fits to the data using eq III, the formalism of Troe. Values of $k_0$ and $k_{inf}$ increase with alkyl substitution on the S atom.

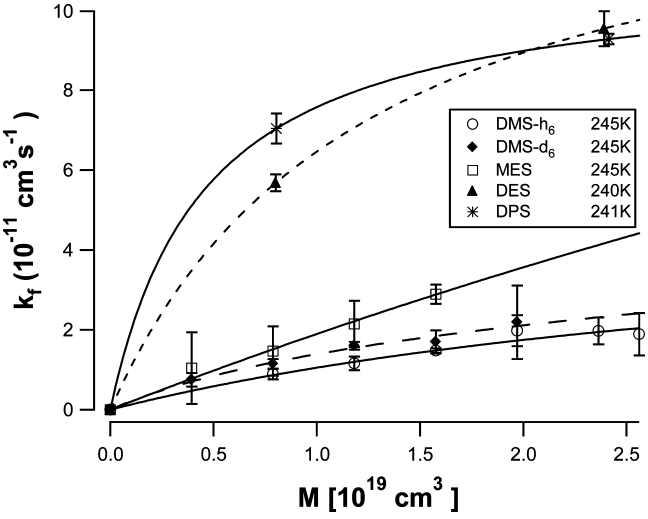


**Figure 13.** Rates of forward addition ($k_{1f-5f}$) plotted as a function of total pressure at temperatures ∼240 K. Values of $k_f$ were determined from fits of eq II to oxygen-dependent data. Solid lines are fits to the data using eq III, the formalism of Troe. Because of the low vapor pressure of DBS, it was not possible to measure reaction 6 as a function of oxygen at temperatures below 261 K.

an increase in the values of $k_0$ as we move from DMS to DBS. At 240 K, DMS, DMS-$d_6$, and MES have similar values, but, unfortunately, we do not have data for DBS.

Assuming that we fit the data sets with a consistent value of $F_c$, we see a trend for $k_\infty$ to increase with molecular complexity. Bock and Ramsey have used photoelectron spectroscopy to study the effect of alkyl substitution on the energy of the nonbonding orbital, which houses the lone pair electrons that participate in the formation of the three electron−two center bond in the adduct.[41] Increasing alkyl substitution raises the energy of the molecular orbital and lowers the ionization energy, and hence it is reasonable to expect some increase in the capture rate of the OH radical, which gives the value of $k_\infty$.

Values for the rate coefficient for the reaction of the adduct with $O_2$ vary from $\sim 6 \times 10^{-13}$ $cm^3 \cdot molecule^{-1} \cdot s^{-1}$ for DMS to $\sim 4 \times 10^{-12}$ $cm^3 \cdot molecule^{-1} \cdot s^{-1}$ for DES, and the faster adduct reaction rate coefficient appears to be responsible for the higher $O_2$ enhancement seen in reaction 4 relative to reaction

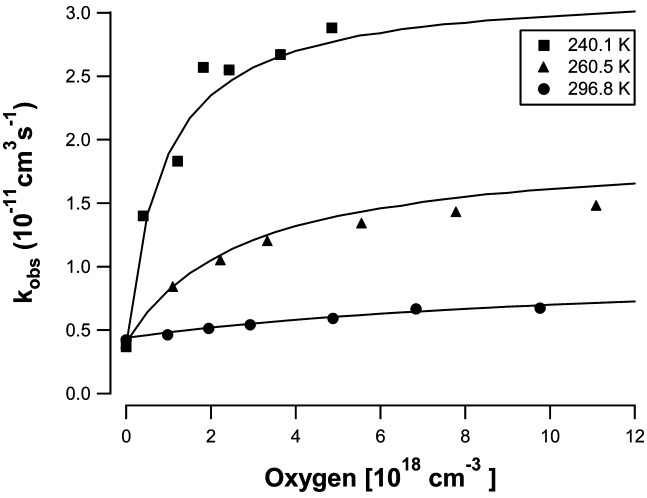


**Figure 14.** Effective rate of Reactions 1 plotted as a function of oxygen partial pressure and a total pressure of ($N_2 + O_2$) of 600 Torr and three different temperatures (240.1, 260.5, and 296.8 K). Solid lines are the predicted rates of oxidation at the respective temperature, oxygen partial pressures, and 600 Torr total pressure using eqs II and VI−IX.

5. It should also be noted that, as discussed above, values of the scavenging rate coefficient are very sensitive to the values of the equilibrium constant that is used. It is possible that the differences in this rate coefficient are an artifact of the use of the DMS van't Hoff parameters to fit all of the sulfide $O_2$ data.

Both theory and experiment present a consistent picture of the detailed mechanism of the $O_2$ enhancement in the OH-initiated oxidation of sulfides. The ab initio calculations show the presence of weakly bound adducts with very similar structures and thermochemistry. This is consistent with our ability to model the $O_2$ enhancements using a single van't Hoff expression and $O_2$ adduct scavenging rate coefficients that are very similar in magnitude. The only significant difference is the falloff behavior of the adduct formation, which, as expected, depends on the size of the molecule.

***2.4. Development of a Predictive Expression for Reactions 1.*** It is now clear that both the effective rate coefficient for the OH-initiated oxidation of alkyl sulfides and the branching ratio between addition and abstraction channels have a complex dependence on temperature, total pressure, and the partial pressure of $O_2$. Prior attempts to describe this complex dependence have utilized empirical fits to a limited amount of experimental data and are valid only at 760 Torr of total pressure. A central goal of this work has been the development of a predictive expression for the effective rate of Reactions 1 under any conditions of atmospheric composition, pressure, and temperature. In addition, the goal has been to base the predictive expression on determinations of the elementary steps in this complex oxidation mechanism. The primary utility of such an expression is the calculation of the effective oxidation rate of DMS, which is entrained into the mid and upper troposphere and may play an important role in particulate formation in these regions. The key difficulty here is that measurements of the adduct equilibration process are only possible at low temperature, and considerable extrapolation, with concomitant uncertainty, is necessary to reach room temperature. In addition the coupled nature of the equilibrium coefficient and scavenging rate coefficient in our fit procedure makes it impossible to extract values of these rate coefficients. The $O_2$ enhancement in $k_{obs}$ is small at 298 K, so $k_f$ is poorly constrained at this temperature. We find that the best global fit to our data for Reactions 1 is obtained by assuming that the rate coefficient for $k_{1s}$ is independent of temperature and pressure with a value of $7 \times 10^{-13}$ cm$^3$·molecule$^{-1}$·s$^{-1}$. If we make this assumption and use our previously determined van't Hoff expression for $K_c$, then we obtain values of $k_{1f}$ that are linearly dependent on pressure between 0 and 600 Torr. Extracting the third-order rate coefficients for reaction 1f,1r and fitting the temperature dependence over the range of 300−240 K gives an expression $k_{1f,third} = 2.9 \times 10^{-31}\,(T/300)^{-6.24}$ cm$^6$·molecule$^{-2}$·s$^{-1}$.

Taking the Arrhenius expression we have obtained, we can use the expressions for $k_a$, $k_f$, $k_s$, and $K_c$ listed below and use them in eq II to obtain the value of $k_{obs}$ for Reactions 1 under any conditions of temperature, pressure, and $O_2$ concentration appropriate to the troposphere.

$$K_c = T \cdot 1.36 \times 10^{-22} \exp(5486/T - 15.601) \quad \text{(VI)}$$

$$k_f = (2.9 \times 10^{-31}(T/300)^{-6.24}\text{cm}^6 \cdot \text{molecule}^{-2} \cdot \text{s}^{-1}) \cdot \text{M} \quad \text{(VII)}$$

$$k_s = 7 \times 10^{-13}\ \text{cm}^3 \cdot \text{molecule}^{-1} \cdot \text{s}^{-1} \quad \text{(VIII)}$$

$$k_a = 7.68 \times 10^{-12}(-167/T)\ \text{cm}^3 \cdot \text{molecule}^{-1} \cdot \text{s}^{-1} \quad \text{(IX)}$$

Figure 14 shows the 600 Torr experimental data at 296, 261,and 240 K together with our predicted fit; the 200 Torr data set is shown in Figure S3. The data are well represented by the fit expression over a wide range of temperature and pressure. We can use this expression for comparisons with the limited number of prior determinations of the $O_2$ dependence of Reactions 1. The predictive expression shows good agreement with the 1986 data of Hynes et al.[4] with the exception of the lowest temperature point at 261 K, and we have discussed the implications of this for the predictive expression in that paper. Barone et al.[7] used a similar approach to our work to study the equilibration of OH with DMS and DMS-$d_6$ and monitored the effective rate coefficient of Reactions 1 as a function of $O_2$ partial pressure in $N_2$ at 100 Torr total pressure at 247 K. Unfortunately, the results are only presented in graphical form; however, our predictive expression appears to underestimate their rate coefficients by 20−30% depending on $O_2$ concentration. The most recent data on Reactions 1 come from Albu et al.,[8] who used a competitive rate technique and measured the effective rate coefficient for Reactions 1 at 760 Torr total pressure over the temperature range of 250−298 K. Measurements were made in $N_2$ buffer gas and with $O_2$ partial pressures of 155 and 380 Torr. Their data are compared with our predictive fit in Table 10. As we have discussed above, there is a significant difference in the measurements in the absence of $O_2$, the abstraction channel. In Figure 15 we show the prediction of the temperature dependence of the $O_2$ enhancement at $O_2$ partial pressures of 155 and 380 at 760 Torr total pressure, the experimental conditions in the study of Albu et al. The experimental points from Albu et al. are in quite good agreement with the predicted enhancement, indicating that the measured $O_2$ enhancement in the relative rate study agrees well with our absolute measurements. This makes the significant difference in the measured abstraction rates more difficult to understand.

## Atmospheric Implications

As we have discussed in prior work, the 1986 predictive expression of Hynes et al. was, until relatively recently, recommended for calculating the temperature dependence of the effective rate coefficients and branching ratios for Reactions 1 in 760 Torr of air, and it was limited to this single pressure.[5]

**TABLE 10: Comparison of the Predicted Rate for the Observed Oxidation of DMS by OH (Reactions 1−1s) with Data of Albu et al.[8] at a Total Pressure of 760 Torr**

| $T$ (K) | pp $O_2$ (Torr) | predicted $k_1$ ($cm^3 \cdot molec^{-1} \cdot s^{-1}$) | Albu et al.[8] |
|---|---|---|---|
| 298 | 0 | $4.39 \times 10^{-12}$ | $(5.0 \pm 1.0) \times 10^{-12}$ |
| | 155 | $6.18 \times 10^{-12}$ | $(7.8 \pm 1.8) \times 10^{-12}$ |
| | 380 | $7.64 \times 10^{-12}$ | $(9.5 \pm 1.9) \times 10^{-12}$ |
| 290 | 0 | $4.32 \times 10^{-12}$ | $(5.7 \pm 1.1) \times 10^{-12}$ |
| | 155 | $7.06 \times 10^{-12}$ | $(9.8 \pm 2.3) \times 10^{-12}$ |
| | 380 | $8.99 \times 10^{-12}$ | $(13.4 \pm 2.7) \times 10^{-12}$ |
| 280 | 0 | $4.23 \times 10^{-12}$ | $(6.2 \pm 1.3) \times 10^{-12}$ |
| | 155 | $8.89 \times 10^{-12}$ | $(12.0 \pm 2.6) \times 10^{-12}$ |
| | 380 | $11.45 \times 10^{-12}$ | $(15.4 \pm 3.1) \times 10^{-12}$ |
| 270 | 0 | $4.14 \times 10^{-12}$ | $(6.3 \pm 1.4) \times 10^{-12}$ |
| | 155 | $11.92 \times 10^{-12}$ | $(15.1 \pm 3.4) \times 10^{-12}$ |
| | 380 | $15.08 \times 10^{-12}$ | $(18.5 \pm 3.7) \times 10^{-12}$ |
| 260 | 0 | $4.04 \times 10^{-12}$ | $(6.4 \pm 1.3) \times 10^{-12}$ |
| | 155 | $16.74 \times 10^{-12}$ | $(19.9 \pm 4.7) \times 10^{-12}$ |
| | 380 | $20.23 \times 10^{-12}$ | $(23.8 \pm 4.7) \times 10^{-12}$ |
| 250 | 0 | $3.94 \times 10^{-12}$ | $(6.6 \pm 1.4) \times 10^{-12}$ |
| | 155 | $23.93 \times 10^{-12}$ | $(28.2 \pm 7.7) \times 10^{-12}$ |
| | 380 | $27.36 \times 10^{-12}$ | $(28.3 \pm 6.2) \times 10^{-12}$ |

In our 2001 work, we were able to show that the 1986 expression underestimated both the effective rate coefficient and the branching ratio in favor of abstraction at low temperatures. The IUPAC panel then recommended a new predictive expression based on a parametrization of this 600 Torr, 240 K data.[34] In recent work, we extended this to develop a predictive expression that would be valid at all pressures at temperatures between 220 and 260 K. With a much larger data set, we have now further extended it to produce an expression that we believe is valid under all conditions of atmospheric pressure and temperature. In Figure 16, we show both the effective rate coefficient and the branching ratio for Reactions 1 as a function of altitude. Rates were calculated using the US standard atmosphere. The branching ratio is defined as the ratio of the abstraction and addition rate coefficients. It can be seen that the effective rate coefficient increases significantly as a function of altitude until we reach the temperature minimum of 216 K at 11 km. At this point, temperature remains constant, but both the pressure and $O_2$ partial pressure continue to decrease, and

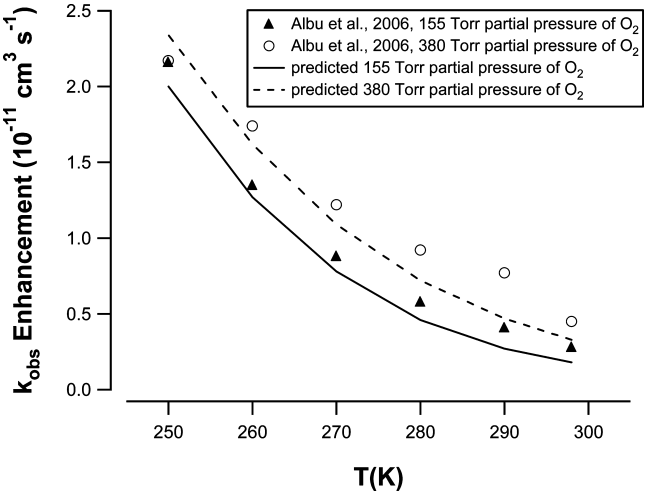


**Figure 15.** Enhancement ($k_{obs} - k_a$) in the effective rate of oxidation for Reactions 1 as measured by Albu et al.[8] at a total pressure of 760 Torr ($N_2 + O_2$) and oxygen partial pressures of 155 and 380 Torr. Solid and dashed lines are the predicted enhancements under those conditions using the expression outlined in Section 2.4.

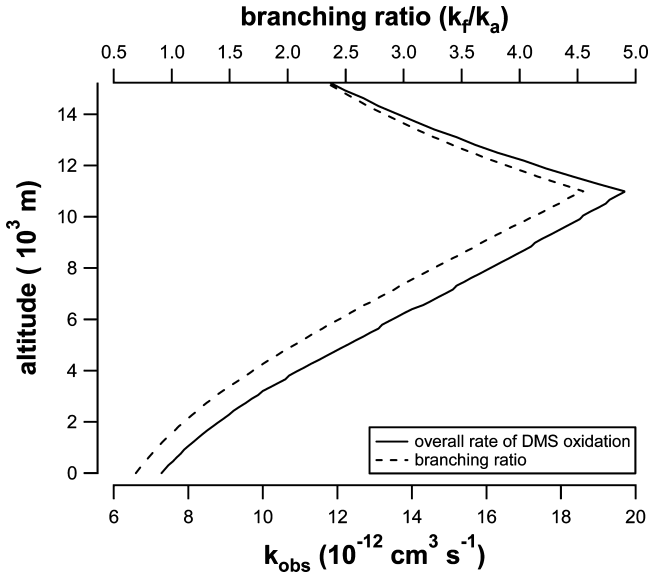


**Figure 16.** Effective rate of DMS oxidation (bottom axis) and the branching ratio between addition and abstraction channels (top axis) plotted against altitude. DMS oxidation is most rapid at an altitude of ~11 000 m and is dominated by the addition channel.

as a consequence, the effective rate coefficient decreases. It can also be seen that above 2 km, reaction proceeds predominantly via the addition channel. Convective uplift of marine boundary layer (MBL) air is a source of DMS to the middle and upper troposphere. The results suggest that DMS will be rapidly oxidized, predominantly by the addition channel at this altitude and that this is a potential route to new particle formation in the mid and upper troposphere.

## Conclusions

We have performed the first theoretical calculations on the dipropyl sulfide and dibutyl sulfide OH adduct species. Geometry optimizations of these molecules were performed, followed by numerical frequency calculations to verify that the adduct structures were minima on the potential-energy hypersurface. The energetics of the reaction of dipropyl sulfide and dibutyl sulfide with OH to form the adduct species were also investigated over a range of temperatures, and these data were compared with prior findings. Our calculations indicate that the strength of the S−O bond increases slightly with the size of the adduct molecule. Our experimental data on reactions 5 and 6 are consistent with these findings. We report the first observations of an oxygen enhancement in the effective rate coefficient for these reactions and find that the enhancement is consistent with the two-channel oxidation mechanism and the elementary rate coefficients used to describe reactions 1−4. We have presented additional data on Reactions 1 and 2 and combine this with previously published data to derive an expression for the effective rate coefficient for DMS oxidation as a function of temperature, pressure, and $O_2$ partial pressure. An analysis of the reactivity trends in the oxidation of the series of alkyl sulfides, reactions 1−6, presents an internally consistent picture of the reaction mechanism, which leads to greatly increased confidence in our use of this mechanism to derive rate coefficients and mechanistic data for the atmospherically important Reactions 1.

**Acknowledgment.** This work was funded by the Office of Naval Research through grant N000149910032.

**Supporting Information Available:** Tables S1a, S1b, S2a, S2b and S3 and Figures S1, S2 and S3 are contained in Supporting Information. This material is available free of charge via the Internet at http://pubs.acs.org.

## References and Notes


(1) Atkinson, R. *Int. J. Chem. Kinet.* **1987**, *19*, 799.

(2) Atkinson, R. *Int. J. Chem. Kinet.* **1986b**, *18*, 555.

(3) Atkinson, R. *Chem. Rev.* **1986**, *85*, 69.

(4) Hynes, A. J.; Stoker, R. B.; Pounds, A. J.; McKay, T.; Bradshaw, J. D.; Nichovich, J. M.; Wine, P. H. *J. Phys. Chem.* **1995**, *99*, 16967.

(5) Hynes, A. J.; Wine, P. H.; Semmes, D. H. *J. Phys. Chem.* **1986**, *90*, 4148.

(6) Williams, M. B.; Campuzano-Jost, P.; Bauer, D.; Hynes, A. J. *Chem. Phys. Lett.* **2001**, *344*, 61.

(7) Barone, S. B.; Tunipseed, A. A.; Ravishankara, A. R. *J. Phys. Chem.* **1996**, *100*, 14694.

(8) Albu, M.; Barnes, I.; Becker, K. H.; Patroescu-Klotz, I.; Mocanu, R.; Benter, T. *Phys. Chem. Chem. Phys.* **2005**, *8*, 728.

(9) Arsene, C.; Barnes, I.; Becker, K.; Mocanu, R. *Atmos. Environ.* **2001**, *35*, 3769.

(10) Arsene, C.; Barnes, I.; Becker, K. H. *Phys. Chem. Chem. Phys.* **1999**, *1*, 5463.

(11) Arsene, C.; Barnes, I.; Becker, K. H.; Schneider, W. F.; Wallington, T. J.; Mihalopoulos, N.; Patroescu, I. *Environ. Sci. Technol.* **2002**, *36*, 5155.

(12) Barnes, I.; Hjorth, J.; Mihalopoulos, N. *Chem. Rev.* **2006**, *106*, 940.

(13) Patroescu, I. V.; Barnes, I.; Becker, K. H.; Mihalopoulos, N. *Atmos. Environ.* **1999**, *33*, 25.

(14) Wallington, T. J.; Atkinson, R.; Tuazon, E. C.; Aschmann, S. M. *Int. J. Chem. Kinet.* **1986**, *18*, 837.

(15) Gonzàlez-García, N.; Gonzàez-Lafont, A.; Lluch, J. M. *ChemPhysChem* **2007**, *8*, 255.

(16) Hynes, A. J. Reaction Mechanisms in Atmospheric Chemistry: Detailed Kinetic and Mechanistic Studies of Hydroxyl Radical Reactions Under Atmospheric Conditions. In *Advances in Spectroscopy: Spectroscopy in Environmental Science*; Clark, R. J. H., Hester, R. E., Eds.; John Wiley & Sons: New York, 1995; Vol. 24, pp 309.

(17) Williams, M. B.; Campuzano-Jost, P.; Pounds, A. J.; Cossairt, B.; Hynes, A. J. *J. Phys. Chem.* **2007**, *111*, 89.

(18) Williams, M. B.; Campuzano-Jost, P.; Pounds, A. J.; Hynes, A. J. *Phys. Chem. Chem. Phys.* **2007**, *9*, 4370.

(19) Barnes, I.; Bastian, V.; Becker, K. H. Kinetic Measurements of OH + Reduced Sulfides. Proceedings of the 9th International Symposium on Gas Kinetics, Bordeaux, France, 1986.

(20) Nielsen, O. J.; Sidebottom, H. W.; Nelson, L.; Rattigan, O.; Treacy, J. J.; O'Farrell, D. J. *Int. J. Chem. Kinet.* **1990**, *22*, 603.

(21) Campuzano-Jost, P.; Williams, M. B.; D'Ottone, L.; Hynes, A. J. *Geophys. Res. Lett.* **2000**, *27*, 693.

(22) D'Ottone, L.; Campuzano-Jost, P.; Bauer, D.; Hynes, A. J. *J. Phys. Chem A* **2001**, *105*, 10538.

(23) Silvente, E.; Richter, R. C.; Hynes, A. J. *J. Chem. Soc., Faraday Trans.* **1997**, *93*, 2821.

(24) Williams, M. B.; Campuzano-Jost, P.; Riemer, D. D.; Tatum, C.; Hynes, A. J. *J. Photochem. Photobiol., A* **2004**, doi: 10.1016/j.photochem.2004.09.008.

(25) Frisch, M. J.; Trucks, G. W.; Schlegel, H. B.; Scuseria, G. E.; Robb, M. A.; Cheeseman, J. R.; Montgomery, J. A., Jr.; Vreven, T.; Kudin, K. N.; Burant, J. C.; Millam, J. M.; Iyengar, S. S.; Tomasi, J.; Barone, V.; Mennucci, B.; Cossi, M.; Scalmani, G.; Rega, N.; Petersson, G. A.; Nakatsuji, H.; Hada, M.; Ehara, M.; Toyota, K.; Fukuda, R.; Hasegawa, J.; Ishida, M.; Nakajima, T.; Honda, Y.; Kitao, O.; Nakai, H.; Klene, M.; Li, X.; Knox, J. E.; Hratchian, H. P.; Cross, J. B.; Bakken, V.; Adamo, C.; Jaramillo, J.; Gomperts, R.; Stratmann, R. E.; Yazyev, O.; Austin, A. J.; Cammi, R.; Pomelli, C.; Ochterski, J. W.; Ayala, P. Y.; Morokuma, K.; Voth, G. A.; Salvador, P.; Dannenberg, J. J.; Zakrzewski, V. G.; Dapprich, S.; Daniels, A. D.; Strain, M. C.; Farkas, O.; Malick, D. K.; Rabuck, A. D.; Raghavachari, K.; Foresman, J. B.; Ortiz, J. V.; Cui, Q.; Baboul, A. G.; Clifford, S.; Cioslowski, J.; Stefanov, B. B.; Liu, G.; Liashenko, A.; Piskorz, P.; Komaromi, I.; Martin, R. L.; Fox, D. J.; Keith, T.; Al-Laham, M. A.; Peng, C. Y.; Nanayakkara, A.; Challacombe, M.; Gill, P. M. W.; Johnson, B.; Chen, W.; Wong, M. W.; Gonzalez, C.; Pople, J. A. *Gaussian 03*, revision C.02; Gaussian, Inc.: Wallingford, CT, 2004.

(26) Frisch, M.; Head-Gordon, M.; Pople, J. *Chem. Phys. Lett.* **1990**, *166*, 275.

(27) Frisch, M.; Head-Gordon, M.; Pople, J. *Chem. Phys. Lett.* **1990**, *166*, 281.

(28) Head-Gordon, M.; Head-Gordon, T. *Chem. Phys. Lett.* **1994**, *220*, 122.

(29) Head-Gordon, M.; Pople, J.; Frisch, M. *Chem. Phys. Lett.* **1988**, *153*, 503.

(30) Ditchfield, R.; Hehre, W. J.; Pople, J. *J. Chem. Phys.* **1971**, *54*, 724.

(31) Raghavachari, K.; Trucks, G. W. *J. Chem. Phys.* **1989**, *91*, 1062.

(32) Ochterski, J. *Thermochemistry in Gaussian*; Gaussian Technical Support Information; Gaussian, Inc.: Wellingford, CT, 2000. Gaussian.com.

(33) Troe, J. *J. Phys. Chem.* **1979**, *83*, 114.

(34) Atkinson, R.; Baulch, D. L.; Cox, R. A.; Crowley, J. N.; Hampson, R. F.; Hynes, R.; Jenkin, M. E.; Rossi, M.; Troe, J. *Atmos. Chem. Phys.* **2006**, *6*, 3625.

(35) Stickel, R. E.; Zhao, Z.; Wine, P. H. *Chem. Phys. Lett.* **1993**, *212*, 312.

(36) Hynes, A. J.; Rosendahl, A. R.; Nien, C. J. OH + DMS: Observations in the Presence of Nitric Acid. Unpublished work, 2003.

(37) Zhao, Z.; Stickel, R. E.; Wine, P. H. *Chem. Phys. Lett.* **1996**, *251*, 59.

(38) Kwok, E. S. C.; Atkinson, R. *Atmos. Environ.* **1995**, *29*, 1685.

(39) Mellouki, A.; Teton, S. T.; LeBras, G. *Int. J. Chem. Kinet.* **1995**, *27*, 791.

(40) Sander, S. P.; Kurylo, M. J.; Orkin, V. L.; Golden, D. M.; Huie, R. E.; Finlayson-Pitts, B. J.; Molina, M. J.; Friedl, R. R.; Ravishankara, A. R.; Moortgat, G. K. *Chemical Kinetics and Photochemical Data for Use in Atmospheric Studies*; JPL Data Evaluation # 14, 02-25 ed.; NASA Jet Propulsion Laboratory: Pasadena, California, 2003.

(41) Bock, H.; Ramsey, B. G. *Angew. Chem., Int. Ed. Engl.* **1973**, *12*, 734.

(42) Burnett, M. N.; Johnson, C. K. ORTEP III: Oak Ridge Thermal Ellipsoid Plot Program for Crystal Structure Illustrations, 1996.


JP9010668